RSC Advances

PAPER

View Article Online
View Journal | View Issue

Cite this: *RSC Adv.*, 2026, **16**, 383

Efficient regeneration of Pd-SSZ-13 catalysts deactivated by alkali metals for passive NO_x adsorption

Dongdong Chen, *[ab] Weiqi Zhang,[a] Zhenzhen Jia,[a] Huibin Liu,[b] Bo Zhang, [a] Shasha Liu,[a] Feng Liang,[a] Wuwan Xiong [a] and Xiang Li*[a]

Received 12th November 2025
Accepted 17th December 2025

DOI: 10.1039/d5ra08741d

rsc.li/rsc-advances

Pd-loaded CHA zeolites (*e.g.*, Pd-SSZ-13) have been identified as a promising candidate for passive NO_x adsorption (PNA) in low-temperature environments. The inclusion of lubricant oil additives or biofuels in automotive exhaust after-treatment systems subjects Pd-SSZ-13 to chemical poisoning from contaminants such as alkali metals (*e.g.*, Na and K). In this study, we present a straightforward yet highly effective approach to regenerate Pd-SSZ-13 that has been poisoned by alkali metals, achieved through washing with a dilute NH_4Cl solution. The underlying mechanisms of both poisoning and regeneration were thoroughly explored, revealing that the deactivation due to alkali-metal poisoning is primarily attributed to the transformation of the active Pd^{2+} ion into PdO_x and a concomitant reduction in Brønsted acid sites. The NH_4Cl washing not only removes alkali metal contaminants, thereby restoring the Brønsted acid sites previously occupied by them, but also converts the inert PdO_x back into their active states (*i.e.*, isolated Pd^{2+}). This investigation unveils a simplified yet highly efficient NH_4Cl washing technique for the regeneration of the deactivated Pd-SSZ-13, offering profound implications for extending the catalyst's lifespan and enhancing its performance in cold-start exhaust after-treatment applications.

1 Introduction

Nitrogen oxides (NO_x) emitted by lean-burn diesel engines represent a substantial environmental threat, contributing to acid rain, photochemical smog and global warming, and their reduction remains particularly challenging in oxygen-rich conditions.[1–3] The selective catalytic reduction of NO_x using ammonia as a reductant (*i.e.* NH_3-SCR) is widely acknowledged as the most effective strategy for NO_x abatement, with high-performance NH_3-SCR catalysts garnering substantial attention.[4–8] However, the formation of NH_3 gas through urea decomposition is impeded at low temperatures during the cold-start phase, thereby limiting the efficacy of NO_x removal.[9,10] Passive NO_x adsorber presents an elegant solution to this challenge by being engineered to adsorb NO_x at temperatures below 200 °C and subsequently release the stored NO_x at elevated temperatures (above 200 °C), aligning with the activation of downstream NH_3-SCR catalytic converters.[9,11–13]

In recent years, the PNA system has garnered substantial scholarly and industrial interest, particularly from automotive manufacturers.[9,11,14–17] In comparison to metal-oxide catalysts (*e.g.*, CeO_2 and Al_2O_3), PNA featuring Pd dispersed on zeolitic supports exhibit remarkable advantages.[18–20] These systems demonstrate superior NO_x adsorption capacity, optimal release temperatures, and exceptional durability under challenging conditions (*e.g.*, SO_2 exposure).[11] Among various zeolite-based materials, Pd-loaded SSZ-13 catalysts (*i.e.*, Pd-SSZ-13) have drawn considerable attention due to their outstanding adsorption efficiency and superior desorption behaviour (typically within the 200–450 °C range).[9,10,13,21] However, under practical operating conditions, catalysts are inevitably compromised by the deposition of alkali metals (*e.g.*, K and Na) from urea solutions and lubricating oil, resulting in their deactivation.[10,17,22,23] The predominant mechanisms of deactivation for Pd-SSZ-13 zeolites by alkali metal poisoning can be extensively outlined as follows:[10,17] (1) isolated Pd sites aggregate into inert bulk PdO_x species, diminishing the number of active sites and reducing the catalyst's reducibility; (2) alkali metal ions replace H^+ in Brønsted acid sites (*i.e.*, Si–OH–Al), resulting in a reduction of the available acidic sites; (3) the zeolite channels and pores are obstructed by aggregated alkali metal oxides and PdO_x species, thereby impairing the catalyst's capacity to eliminate low-temperature NO_x.

[a]*School of Environmental and Chemical Engineering, Guangdong Provincial Key Laboratory of Environmental Health and Land Resource, Zhaoqing University, 526061 Zhaoqing, China. E-mail: chendongdong@zqu.edu.cn*

[b]*National Engineering Laboratory for VOCs Pollution Control Technology and Equipment, Guangdong Provincial Key Laboratory of Atmospheric Environment and Pollution Control, School of Environment and Energy, South China University of Technology, 510006 Guangzhou, China*

The replacement of a depleted PNA catalyst proves economically untenable due to the exorbitant costs associated with both the precious metal Pd and the SSZ-13 zeolitic support. Consequently, catalyst regeneration emerges as a crucial strategy for revitalizing deactivated PNA materials, presenting a pragmatic solution to extend their operational lifespan while mitigating the environmental issues associated with the disposal of exhausted catalysts.[24] As previously highlighted, alkali metal ions tend to occupy the ion-exchanged sites, thereby converting Pd^{2+} ions into inert bulk PdO_x. Therefore, during the regeneration of alkali-metal-poisoned Pd-SSZ-13 samples, it is imperative not only to remove the alkali metals that occupy the Brønsted acid sites but also to dismantle the PdO_x aggregates, facilitating their reversion to the ion-exchange sites, where they can reform into active, isolated Pd^{2+} ions. To the best of our knowledge, technical methodologies for regenerating Pd-SSZ-13 catalysts compromised by alkali metal ion poisoning remain largely unexplored. Thus, research in this area is of substantial scientific and practical significance, offering prospective solutions to the pressing challenges associated with the regeneration of catalysts impacted by alkali metal ion contamination. It is well documented that bulk PdO_x can be reverted to Pd ions through hydro/hydrothermal treatment;[24–26] however, alkali metal ions remain resistant to removal *via* such methods due to the robust interaction between the alkali metal ions and the exchange sites within the zeolitic structure.[27] Recent studies have demonstrated that alkali-metal-poisoned Cu-loaded zeolites can be regenerated by washing with a diluent solution containing NH_4^+ ions.[27–29] This raises an intriguing and important question: could NH_4^+ exert similar positive effects on the regeneration of more costly alkali-metal-poisoned PNA catalysts, such as Pd-SSZ-13, which hold considerable potential in addressing the cold-start NO_x emission issue?

In this investigation, a series of Pd-SSZ-13 catalysts, rendered inactive by alkali metal poisoning (K and Na), were synthesized using an impregnation methodology. The regeneration of these poisoned catalysts was successfully achieved through the implementation of a robust strategy involving the washing with a dilute NH_4Cl solution. To comprehensively elucidate the deactivation and regeneration mechanisms of Pd-SSZ-13, a wide array of characterization techniques (XRD, N_2-physisorption, DR UV/Vis, H_2-TPR, NH_3-TPD, SEM, TEM, XPS, ^{27}Al solid-state NMR, NO- and NH_3-DRIFT) was employed to investigate the physicochemical, structural, acidic, Pd-speciation properties, as well as the alkali metal (*e.g.*, Na and K) species of the fresh, poisoned, and regenerated catalysts. The outcomes of this investigation possess significant practical relevance, as they offer a successful approach to regenerate the catalytic activity of alkali-metal-poisoned Pd-based catalysts.

2 Materials and methods

2.1 Catalyst synthesis

The pristine proton-type SSZ-13 zeolite (H-SSZ-13, $SiO_2/Al_2O_3 = 11$) was procured from Dalian Zhuoran Environmental Protection Co., Ltd (P. R. China). Palladium nitrate dihydrate ($Pd(NO_3)_2 \cdot 2H_2O$, Pd $\geq$ 39.0%) and ammonium sulfate ($(NH_4)_2SO_4$, 99 wt%) were sourced from Shanghai Aladdin Biochemical Technology Co., Ltd (P. R. China). Potassium nitrate (KNO_3) and sodium nitrate ($NaNO_3$) were purchased from Guangzhou Chemical Reagent Factory.

A Pd-SSZ-13 catalyst, incorporating 1 wt% Pd, was synthesized *via* an impregnation method, utilizing the commercially acquired H-SSZ-13 as the zeolitic support. In the typical procedure, 500 mL of 1 M $(NH_4)_2SO_4$ aqueous solution was combined with 10 g of the H-type zeolite support and stirred at ambient temperature for 1 hour.[30] After washing by deionized water for three times, the products were recovered by filtered and dried by an oven at 200 °C to yield ammonia-type SSZ-13 (labeled as NH_4-SSZ-13).[30] The NH_4-SSZ-13 was subsequently impregnated with palladium nitrate dihydrate to prepare palladium-modified SSZ-13 (*i.e.* Pd-SSZ-13) with a 1 wt% Pd loading. The wetted precursor was dried at ambient temperature for 24 hours, followed by further drying at 60 °C for 12 hours. Finally, the catalyst underwent calcination at 550 °C for 4 hours, resulting in the fresh Pd-SSZ-13 catalysts, denoted as Pd-Z-F. The K- or Na-modified Pd-SSZ-13 catalysts were prepared by impregnating the Pd-Z-F sample with a specific quantity of $NaNO_3$ or KNO_3 solution, targeting a theoretical alkali metal loading of 1 mmol g^{-1}. The mixture was left to equilibrate at ambient temperature for 24 hours, after which it was dried overnight and calcined in flowing air at 500 °C at a rate of 5 °C min^{-1} for 4 hours, resulting in the successful synthesis of Na- and K-poisoned Pd-SSZ-13 catalysts, labeled as Pd-Z-Na and Pd-Z-K, respectively.

The regeneration of Pd-SSZ-13 catalysts, poisoned by alkali metals, was effectuated through treatment with a dilute NH_4Cl solution as outlined in recent literatures.[27,28] Specifically, 2.0 g of the alkali-metal-contaminated catalysts (Pd-Z-Na and Pd-Z-K) were mixed with 400 mL of 0.01 M NH_4Cl solution and agitated at 80 °C for 1 hour. Subsequent to filtration, the catalysts were thoroughly rinsed with deionized water and subjected to drying at 110 °C in an oven. The regenerated Pd-Z-Na and Pd-Z-K catalysts were subsequently recovered, designated as Pd-Z-Na-R and Pd-Z-K-R, respectively.

2.2 Catalyst characterization

The crystalline structure of the zeolite samples was examined *via* powder X-ray diffraction (XRD) using a Bruker D8-Advance diffractometer, utilizing Cu Kα radiation with a scan rate set to 5° min^{-1}. The specific surface areas and the pore volumes of the catalysts were determined by nitrogen adsorption/desorption tests, employing the Brunauer–Emmett–Teller (BET) method on an ASAP 2020 analyzer at 77 K. Diffuse reflectance ultraviolet-visible (DR UV/Vis) spectroscopy was conducted on a Lambda 650 spectrometer (PerkinElmer) equipped with an integrating sphere, with $BaSO_4$ serving as the reference standard. SEM measurements were performed on an ultra-high resolution field emission scanning electron microscope (SU8600, Hitachi). TEM images and EDX mappings were collected using a transmission electron microscope (Tecnai G2 F20, FEI) at an accelerating voltage of 200 kV. Hydrogen temperature-programmed reduction (H_2-TPR) and ammonia

temperature-programmed desorption (NH_3-TPD) analyses were carried out on a BSD-Chem C200 apparatus. For each H_2-TPR test, approximately 50 mg of the zeolite sample was placed in a U-type quartz tube, and the temperature was elevated from 45 °C to 700 °C, with 10 vol% H_2/Ar serving as the carrier gas. The NH_3-TPD procedure involved pre-treating 50 mg of the catalyst powder at 550 °C for 1 hour in a helium flow to eliminate adsorbed moisture and impurities, followed by cooling to 50 °C. Subsequently, the catalyst was exposed to 10 vol% NH_3 in He for 1 hour to achieve surface saturation. After purging with He for 60 minutes to remove both gaseous and physically adsorbed NH_3, the temperature was ramped from 50 °C to 700 °C at 10 °C min^{-1} to record the NH_3-TPD profile. Surface composition analysis was performed *via* XPS utilizing an ESCALAB 250 system (Thermo Fisher Scientific, USA), equipped with a monochromatic Al Kα X-ray source ($h\nu = 1486.8$ eV). The binding energy calibration was achieved by referencing the C 1s peak at 284.6 eV. Solid-state ^{27}Al Nuclear Magnetic Resonance (NMR) spectra were acquired on a Bruker Avance III 600 MHz spectrometer equipped with a 4.0 mm CP MAS probe, calibrated at 12 kHz MAS frequency. For NMR analysis, $Al(NO_3)_3$ (1 M) solution was utilized as a reference for the chemical shifts of ^{27}Al. The relative concentrations of alkali metals were determined using inductively coupled plasma optical emission spectroscopy (ICP-OES, Agilent 720, USA). *In situ* diffuse reflectance Fourier-transform infrared (DRIFT) spectra were recorded using a Bruker INVENIO R spectrometer, equipped with a dedicated reaction chamber featuring ZnSe optical windows and a Harrick Praying Mantis mirror assembly for enhanced diffuse reflection. Spectral data were collected over a wavenumber range of 4000 to 650 cm^{-1}, with a spectral resolution of 2 cm^{-1}, averaging 32 scans per measurement to optimize signal quality. To establish a linear correlation between surface concentration and infrared band intensity, data were processed using the Kubelka–Munk (KM) method. Prior to measurements, the sample was pretreated at 500 °C for 1 hour in a flowing air atmosphere. Background spectra were recorded after cooling to the target temperature, and two distinct sets of DRIFTS data were obtained: (i) NO as the probe molecule adsorbed on the zeolites at 100 °C; (ii) NH_3 at 25 °C.

2.3 Catalyst evaluation

The NO_x adsorption and desorption behaviors of the fresh, poisoned and regenerated Pd-SSZ-13 catalysts were evaluated using a custom-designed continuous-flow quartz reactor. For each standard NO_x adsorption/desorption measurement, 50 mg of the prepared catalyst (sieved to 40–60 mesh) was used. Prior to testing, the catalysts were subjected to pretreatment at 500 °C for 60 minutes in an air stream, followed by natural cooling to target reaction temperature (*i.e.* 100 °C) without altering the gas composition. The adsorption process began immediately after introducing 200 ppm NO_x, 200 ppm CO (when required), and 3 vol% H_2O (when required) into the gas stream. The samples were held at 100 °C for approximately 10 minutes to facilitate NO_x uptake. Subsequently, the furnace temperature was ramped from 100 to 600 °C at 10 °C per minute to assess NO_x desorption. Throughout the experiment, effluent gases and their concentrations were continuously monitored using an online FT-IR spectrometer (MKS MultiGas 6030), equipped with a heated gas cell maintained at 191 °C.

3 Results and discussions

3.1 NO_x adsorption/desorption properties of Pd-SSZ-13 catalysts

To explore the potential for regenerating Pd-SSZ-13 catalysts poisoned by alkali metal ions through washing with NH_4Cl solution, the NO_x adsorption/desorption characteristics of Pd-Z-F, Pd-Z-Na, Pd-Z-K, Pd-Z-Na-R and Pd-Z-K-R catalysts, both in the presence and absence of CO and H_2O, were evaluated, the results are illustrated in Fig. 1 and S1. It is widely recognized that the negative peak at low temperatures in the NO_x adsorption/desorption profiles corresponds to the NO_x storage capacity, whereas the positive peaks at elevated temperatures signify the NO_x desorption capacity. As anticipated, the PNA performance of the alkali-metal-ion-poisoned Pd-SSZ-13, with 1 mmol g^{-1} of Na or K, exhibited a significant decline. Specifically, prior to the addition of CO and H_2O (Fig. 1a and S1a), the total adsorption capacity of the unpoisoned Pd-Z-F sample diminished from 131.79 μmol g^{-1} to 22.32 μmol g^{-1} and 17.86 μmol g^{-1} for the poisoned Pd-Z-Na and Pd-Z-K samples, respectively. Upon washing with NH_4Cl solution, the detrimental impact of alkali metals on the NO_x storage capacity of Pd-SSZ-13 was almost completely eliminated, and the NO_x desorption capacity of the regenerated Pd-Z-Na-R and Pd-Z-K-R catalysts increased to 129.46 μmol g^{-1} and 127.32 μmol g^{-1}, respectively. It has been reported that desorption peaks below 200 °C, which are only observable under dry conditions, are indicative of weakly bound NO_x on Brønsted acid sites, $Pd(OH)^+$ species, or bulk PdO_x. These results suggest that both K and Na ions contribute significantly to the loss of Brønsted acid and Pd^{2+} sites. However, almost all of these lost sites were recovered following NH_4Cl solution washing. To more accurately simulate real-world conditions, the feed gas was subsequently enriched with 3 vol% H_2O and 200 ppm CO. The resulting NO_x adsorption/desorption properties of the five Pd-SSZ-13 catalysts are presented in Fig. 1b and S1b. It has been demonstrated that NO_x adsorption onto Pd-SSZ-13 is hindered under wet conditions due to the occupation of partial Pd^{2+} and Brønsted acid sites by H_2O molecules.[9] Nevertheless, CO mitigates the negative influence of H_2O by reacting with NO to form NO–Pd(II)–CO species (Fig. S2).[9] As observed in Fig. 1b and S1b, the total adsorption capacity of the Pd-Z-F sample decreased from 56.90 μmol g^{-1} to 15.71 μmol g^{-1} and 14.72 μmol g^{-1} for the poisoned Pd-Z-Na and Pd-Z-K samples, respectively. Following NH_4Cl washing, the NO_x adsorption capacity increased to 46.66 μmol g^{-1} and 43.37 μmol g^{-1} for the regenerated Pd-Z-Na-R and Pd-Z-K-R catalysts, respectively. Furthermore, unlike the dry condition, the NO_x adsorption/desorption profiles of all samples under CO and H_2O conditions exhibited a broad desorption peak above 350 °C, attributed to the stabilization of NO_x by isolated cationic Pd sites.[9,12] As shown in Fig. 1b and S1b, the intensity of the desorption peak above 350 °C was significantly

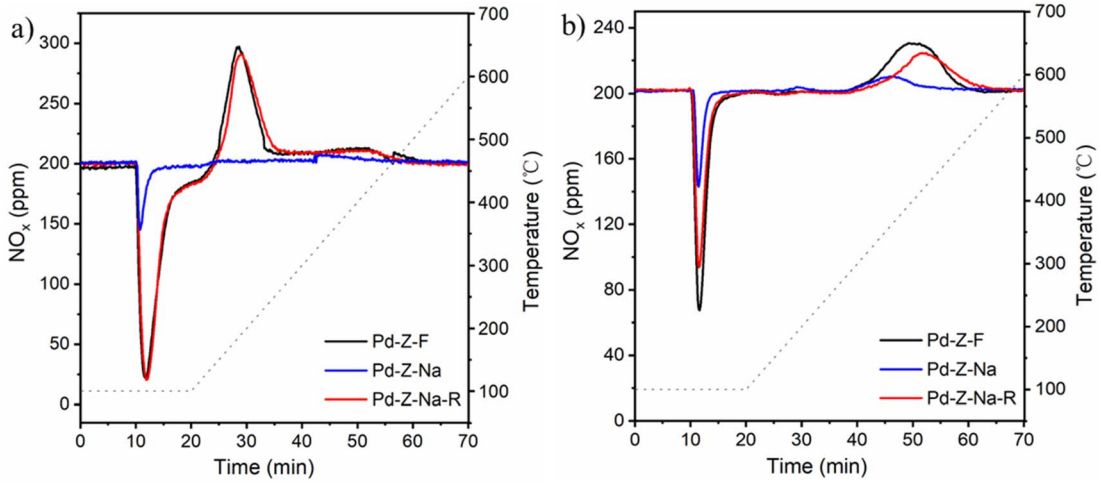

Fig. 1 PNA performances of fresh Pd-Z-F, Na-poisoned Pd-Z-Na and the regenerated Pd-Z-Na-R catalysts under different conditions. (a) Gas feed: 200 ppm of NO_x and 10 vol% O_2 in N_2; (b) gas feed: 200 ppm of NO_x, 200 ppm of CO, 3 vol% H_2O and 10 vol% O_2 in N_2. Samples were treated at 500 °C in 10 vol% O_2 for one hour before all the tests, and a total flow rate of 200 mL min^{-1} was used.

reduced after K or Na poisoning, which was due to the loss of isolated Pd^{2+} sites. After washing with NH_4Cl solution, the peak intensity above 350 °C increased, indicating the recovery of the active Pd^{2+} sites. A more detailed discussion of the NO_x adsorption activity of the poisoned and regenerated catalysts will follow, integrated with characterizations of the Pd active sites and surface acid sites.

3.2 Characterizations of the catalysts

The surface morphology and porosity of the catalysts were rigorously scrutinized through FE-SEM, with the corresponding data presented in Fig. S3. FE-SEM imaging revealed the retention of cubic particle morphology across all synthesized samples, with no significant morphological change observed following alkali-metal-poisoning and regeneration (Fig. S3). Nitrogen physisorption techniques was conducted to investigate the specific surface areas and porosity information, the results are shown in Fig. 2, S4 and Table S1. Prior to poisoning, the Pd-Z-F catalyst exhibits a specific surface area of 536.05 $m^2 g^{-1}$ and a micropore volume of 0.233 $cm^3 g^{-1}$. Post-poisoning, the specific surface area and micropore volume of the Pd-Z-Na catalyst drop to 497.89 $m^2 g^{-1}$ and 0.205 $cm^3 g^{-1}$, respectively, while those of the Pd-Z-K catalyst decrease to 487.14 $m^2 g^{-1}$ and 0.209 $cm^3 g^{-1}$, which can be attributed to pore blockage from newly formed PdO aggregates and alkali metal oxides. Following regeneration, the specific surface area and micropore volume of the Pd-Z-Na-R catalyst exhibited an increase to 505.74 $m^2 g^{-1}$ and 0.216 $cm^3 g^{-1}$, respectively, while the Pd-Z-K-R catalyst showed improvements to 498.28 $m^2 g^{-1}$ and 0.224 $cm^3 g^{-1}$. These enhancements are likely attributed to the conversion of PdO aggregates back into isolated Pd^{2+} species, thereby relieving the pore blockage and restoring the catalyst's porosity.

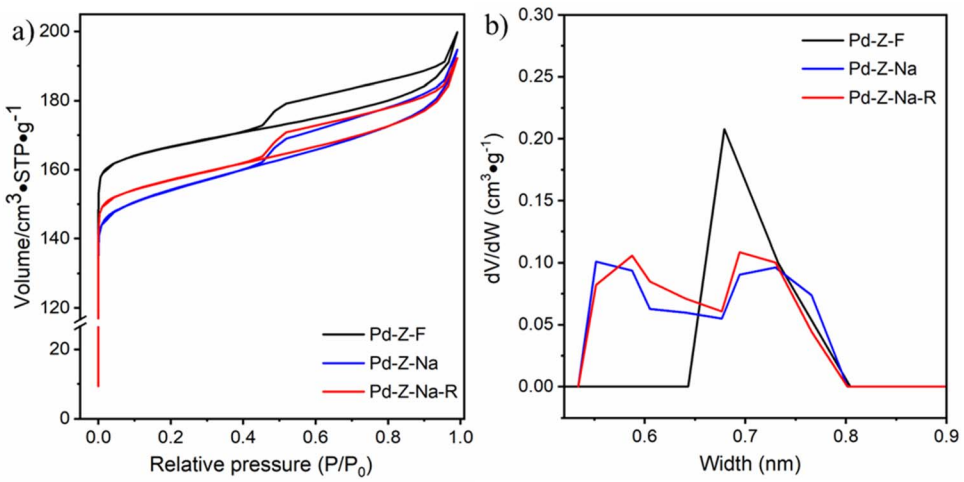

Fig. 2 N_2-physisorption curves (a) and micropore size distributions (b) analyzed by the NLDFT method for Pd-Z-F, Na-poisoned Pd-Z-Na and the regenerated Pd-Z-Na-R catalysts.

The structural characteristics of the catalysts were meticulously probed *via* XRD and ^{27}Al MAS NMR analyses, with the corresponding datasets illustrated in Fig. 3, S5 and S6. As depicted in Fig. 3a and S5a, all catalysts preserved their intrinsic CHA frameworks following exposure to Na- and K-induced deactivation and subsequent regeneration, indicating that the long-range ordered zeolitic architectures remain largely unperturbed.[31] Notably, the intensities of the hallmark diffraction peaks corresponding to the chabazite structure in alkali-metal poisoned Pd-Z-Na and Pd-Z-K catalysts were markedly attenuated relative to the pristine Pd-Z-F, attributable to the deposition of alkali metal species predominantly on the support surface, which exerts a deleterious effect on the structural peaks.[10,17] Intriguingly, subsequent NH_4Cl washing restored the peak intensities of Pd-Z-Na-R and Pd-Z-K-R to levels comparable with Pd-Z-F, underscoring the efficacy of the regeneration process. Moreover, Fig. 3b and S5b reveal that the diffraction peak at $2\theta = 33.9°$, associated with PdO species, exhibits an inverse trend relative to the chabazite peaks in alkali-metal poisoned Pd-Z-Na and Pd-Z-K, compared with the fresh catalyst. This observation suggests that alkali-metal poisoning promotes the formation of PdO nanoparticles. Upon NH_4Cl-mediated regeneration, the intensity of the $2\theta = 33.9°$ peak diminished relative to the poisoned samples, implying the reconversion of aggregated PdO species into catalytically active, isolated Pd^{2+} ions.[32–35] Complementary insights into the structural perturbations were obtained through ^{27}Al MAS NMR spectroscopy, providing further evidence of framework integrity of the catalysts. Notably, in Fig. S6, the Pd-Z-F catalyst exhibits a prominent peak at 58 ppm, alongside a subtle peak at 0 ppm, corresponding to tetrahedrally coordinated framework Al and six-coordinated extra-framework aluminum Al, respectively.[22,31,36] In comparison to the Pd-Z-F catalyst, the peaks corresponding to the framework Al slightly broaden in the Pd-Z-K and Pd-Z-Na catalysts, aligning with previous studies.[10] Moreover, the intensity of the six-coordinated extra-framework

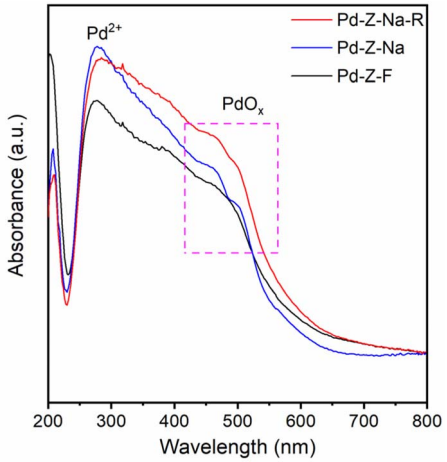

Fig. 4 DR UV/Vis spectra of Pd-Z-F, Na-poisoned Pd-Z-Na and the regenerated Pd-Z-Na-R catalysts.

Al diminishes post-poisoning, attributable to the interaction of alkali metals with these Al sites, forming NMR-invisible species such as $KAlO_2$ (or $NaAlO_2$) or the highly disordered undetectable Al species.[22,37] Upon regeneration *via* NH_4Cl washing, the deleterious impact of alkali metal contamination is substantially mitigated.

DR UV/Vis spectroscopy was employed to examine the coordination environment and oxidation state of Pd species in the freshly synthesized Pd-SSZ-13 catalysts, with the results illustrated in Fig. 4 and S7. As illustrated in Fig. 4, the spectrum of the Pd-Z-F catalyst displays a distinct absorption band within the 200 to 300 nm range, which is ascribed to charge transfer interactions between Pd and the oxygen ligands.[9,24] This observation suggests that Pd^{2+} ions represent the predominant palladium species in the non-poisoned sample. Both Fig. 4 and S7 demonstrate a broad, pronounced shoulder between 400 and 500 nm after Na or K poisoning, in contrast to the Pd-Z-F

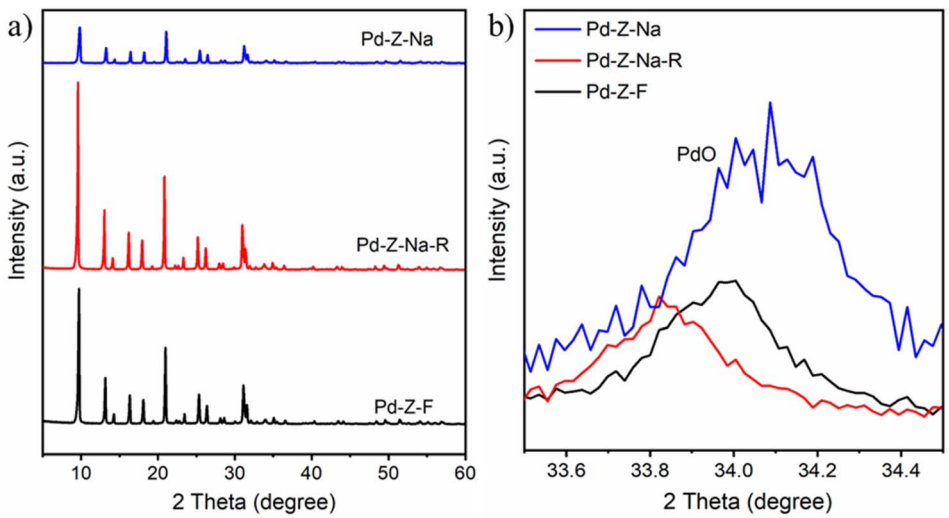

Fig. 3 (a) XRD patterns of Pd-Z-F, Na-poisoned Pd-Z-Na and the regenerated Pd-Z-Na-R catalysts. (b) Enlarged XRD patterns (normalized to the intensity of main band at $2\theta = 9.6°$ in the respective spectrum) in 33.5–34.5°.

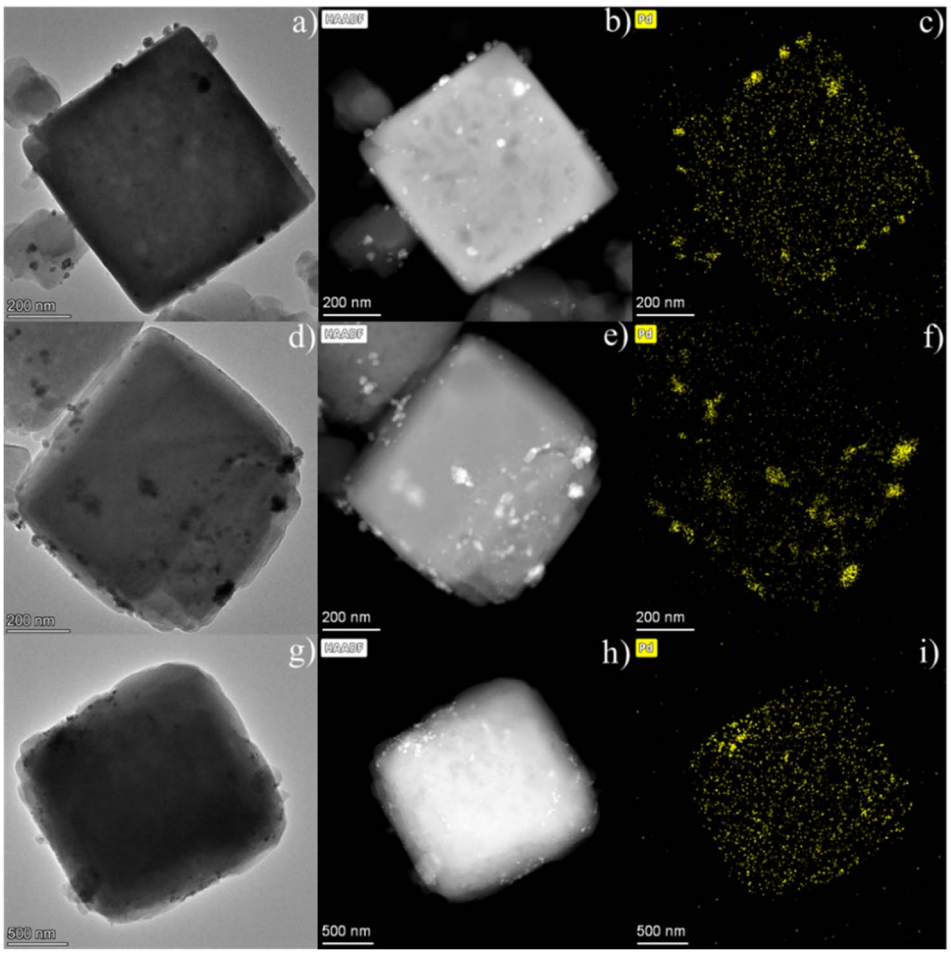

Fig. 5 (a, d and g) TEM, (b, e and h) HAADF-STEM images, and (c, f and i) EDX mapping of Pd for Pd-Z-F (panels (a–c)), Pd-Z-Na (panels (d–f)) and Pd-Z-Na-R (panels (g–i)) catalysts.

catalyst. This feature is attributed to the characteristic electronic transitions of Pd^{2+} within a tetragonally coordinated oxygen environment (*i.e.*, PdO_x).[9,21,24] The proliferation of PdO_x aggregates can be ascribed to the propensity of alkali metals to perturb the interactions between the metal ion-active sites (*e.g.*, Pd^{2+} and Cu^{2+}), thereby fostering the mobilization of these cationic species and catalyzing the coalescence into aggregated PdO_x or CuO_x structures.[17,38,39] Nonetheless, NH_4Cl washing can convert the bulk PdO_x, which is caused by alkali metal poisoning, back into ionic Pd species. Specifically, as illustrated in Fig. 4 and S7, Pd-Z-Na-R and Pd-Z-K-R catalysts display an enhanced peak in the 200–300 nm range and a reduced peak in the 400–500 nm range compared to their poisoned counterparts, indicating that a fraction of PdO_x can be reverted to the active Pd^{2+} form post NH_4Cl washing treatment.

HAADF-STEM imaging, accompanied by EDX mapping, was employed to elucidate the spatial distribution of Si, Al, O, and Pd in both the poisoned and regenerated Pd-SSZ-13 catalysts, with particular focus on the distribution of Pd following the poisoning and regeneration processes. The other elements (Si, Al, O) in all catalysts are observed to be distributed uniformly, however, the state of the Pd element varied significantly among the different catalysts (Fig. S8). Specifically, the STEM (TEM) and EDX mapping images (Fig. 5a–c) of the Pd-Z-F sample clearly depict the formation of a moderate quantity of Pd nanoparticles on the zeolite surface, while the majority of Pd species remain extensively dispersed within the CHA cages. However, following alkali-metal poisoning, significantly larger Pd-containing aggregates (up to tens of nanometers in size) were observed on the zeolitic surface, as shown in Fig. 5d, e and S9a–c. This observation unequivocally substantiates that alkali metal ions occupy the exchanged sites, promoting the formation of bulk PdO particles on the zeolite surface. After regeneration *via* NH_4Cl solution washing, a marked reduction in the number of Pd nanoparticles on the external surface of Pd-Z-Na-R and Pd-Z-K-R zeolites was noted, and the EDX mapping images of Pd revealed a homogenous distribution (Fig. 5g–i and S9d–f). This suggests that NH_4Cl promotes the conversion of PdO aggregates, newly generated due to alkali metal poisoning, into isolated Pd cations. Furthermore, NH_4Cl washing effectively removes K and Na ions from the Pd-SSZ-13 system, thereby reinstating the Brønsted acid sites that were previously occupied by these alkali-metal ions. The removal of alkali-metal ions is confirmed through elemental distribution analysis *via*

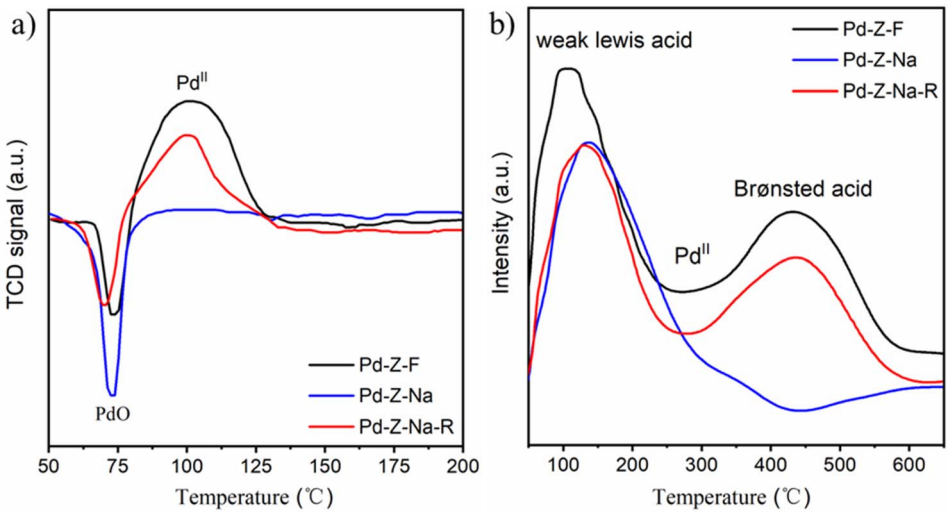

Fig. 6 H_2-TPR curves (a) and NH_3-TPD profiles (b) of Pd-Z-F, Na-poisoned Pd-Z-Na and the regenerated Pd-Z-Na-R catalysts.

EDX mapping of Na and K (Fig. S10) as well as high-resolution XPS of the Na 1s and K 2p spectra (Fig. S11). Remarkably, as shown in Fig. S10, substantial amounts of K and Na ions are detected in the Pd-Z-Na and Pd-Z-K catalysts, respectively. However, most of these ions are effectively removed after NH_4Cl treatment. The XPS spectra of Pd-Z-Na-R and Pd-Z-K-R in Fig. S11 further confirm that the alkali-metal ions are successfully eliminated from the poisoned Pd-SSZ-13 catalysts after regeneration. Consistent with these findings, the ICP-OES results in Table S2 show that the Na content decreases from 1.55% in Pd-Z-Na to 0.11% in Pd-Z-Na-R, and the K content decreases from 1.99% in Pd-Z-K to 0.50% in Pd-Z-K-R following NH_4Cl washing.

To examine the transformation of Pd species under Na or K poisoning and their subsequent regeneration in Pd-SSZ-13, H_2-TPR experiments were performed to characterize the diverse Pd species according to their specific reduction temperature profiles. The data, presented in Fig. 6a and S12a, reveal a distinct broad positive H_2 consumption peak spanning 80 °C to 140 °C, attributed to the reduction of Pd^{2+} ions, prominently observed in the Pd-Z-F catalyst, indicating a significant concentration of Pd^{2+} ions within the material.[9,10,24,33] Furthermore, a sharp negative H_2 desorption peak near 72 °C was also detected in the Pd-Z-F catalyst, pointing to the existence of a small quantity of PdO.[9,10,24,33] Upon Na poisoning, the intensity of the positive peak linked to Pd^{2+} ions in the Pd-Z-Na catalyst diminishes substantially, while the negative peak associated with PdO becomes markedly more intense, suggesting a pronounced aggregation of isolated Pd^{2+} species driven by Na-induced poisoning (Fig. 6a). These findings indicate that alkali metals poisoning facilitate the conversion of Pd^{2+} ions into bulk PdO, aligning with the conclusions of Li *et al.*[10] Interestingly, as illustrated in Fig. 6a, the intensity of the PdO peak in the Pd-Z-Na-R catalyst experiences a marked reduction, while the signal corresponding to Pd^{2+} ions undergo a substantial enhancement. This observation underscores the efficacy of washing with a dilute NH_4Cl solution in converting bulk PdO back into its active, isolated Pd^{2+} ionic form. To further substantiate this phenomenon, the K-poisoned and regenerated Pd-SSZ-13 catalyst (*i.e.*, Pd-Z-K and Pd-Z-K-R) were also subjected to H_2-TPR analysis, as depicted in Fig. S12a. Remarkably, the PdO species previously present in the Pd-Z-K sample were nearly entirely eliminated, and the peak intensity corresponding to the active Pd^{2+} ions was mostly restored in the Pd-Z-K-R catalyst. This validates the regeneration mechanism involving NH_4Cl washing as highly effective for mitigating both Na and K-induced poisoning.

To elucidate the impact of alkali metal ions on the acidic characteristics of Pd-SSZ-13, NH_3-TPD experiments were conducted to probe the alterations in the material's acidity before and after exposure to a dilute NH_4Cl solution. The data, presented in Fig. 6b and S12b, disclose three distinct NH_3 desorption peaks for the Pd-Z-F catalyst. The initial peak, observed at temperatures below 200 °C, indicates NH_3 adsorption on weak Lewis acid sites, such as surface hydroxyl groups and aluminum species located outside the zeolite framework.[9,22,31,36] The additional peaks at about 275 °C and 430 °C correspond to NH_3 desorption from medium and strong acid sites.[9,22,31,36] These peaks are attributed to the release of NH_3 from cationic Pd^{2+} species at the zeolite exchange sites (*i.e.*, stronger Lewis acid sites) and Brønsted acid sites, respectively, thus emphasizing the presence of both acidic functionalities within the Pd-Z-F catalyst.[9,22,31,36] As indicated in Table S3, upon Na or K poisoning, the intensities of all NH_3 desorption peaks in the poisoned Pd-Z-Na and Pd-Z-K samples diminished significantly as compared to Pd-Z-F sample, particularly those associated with medium and strong acid sites. This suggests that both K^+ and Na^+ ions induce a reduction in the number of active Pd^{2+} and Brønsted acid sites. Notably, the Brønsted acid sites in the Pd-Z-Na and Pd-Z-K catalysts almost entirely vanish due to the occupation by K^+ and Na^+ ions, respectively. Following washing with a dilute NH_4Cl solution, the NH_3 desorption peaks of the regenerated Pd-Z-Na-R and Pd-Z-K-R catalysts were nearly restored to levels akin to those of the pristine Pd-Z-F

catalyst, implying that the previously occupied Brønsted acid sites were liberated. This restoration is attributed to the ability of NH_4^+ ions to effectively displace K^+ and Na^+ ions *via* ion-exchange, a conclusion that is corroborated by the high-resolution K 1s and Na 1s XPS spectra shown in Fig. S11.

NO can be adsorbed onto Pd cations situated at exchanged sites in Pd-SSZ-13 in the absence of H_2O, yielding distinguishable FT-IR spectra. Consequently, DRIFTS experiments utilizing NO as a probe molecule (*i.e.* NO-DRIFTS) were conducted to investigate the alterations in Pd states within the Pd-SSZ-13 catalysts post-poisoning and regeneration. The FT-IR spectra obtained upon NO adsorption on fresh, alkali-metal-poisoned, and regenerated catalysts are presented in Fig. 7, S13 and S14. Two prominent FT-IR bands at 1857 and 1818 cm^{-1} were observed in Pd-Z-F prior to poisoning, attributed to the ν(NO) vibrations of Pd^{2+}–NO and $Pd(OH)^+$–NO, respectively.[9,12,40] It is postulated that two distinct divalent Pd^{2+} species are involved: isolated Pd^{2+} species coordinated with two adjacent Al sites in six-membered ring (6MR) units and $Pd(OH)^+$ species stabilized by individual Al sites in eight-membered ring (8MR) units.[9,32,41] Previous studies have suggested that the formation of $Pd(OH)^+$–NO and Pd^{2+}–NO arises from the adsorption of NO on isolated $Pd(OH)^+$ and Pd^{2+} cations, respectively.[12,32,40,41] Thus, the relative intensities of the peaks at 1818 and 1857 cm^{-1} can be correlated with the relative abundance of $Pd(OH)^+$ and Pd^{2+} in the Pd-SSZ-13 catalysts.[32] As indicated in Fig. 7 and S13, compared to the Pd-Z-F sample, the NO adsorption IR peaks at 1818 and 1857 cm^{-1} are nearly absent after Na or K poisoning, signaling the near-total disappearance of Pd cations in both the poisoned Pd-Z-Na and Pd-Z-K samples. However, after treatment with NH_4Cl solution, the NO adsorption peaks at 1818 and 1857 cm^{-1} in the Pd-Z-Na-R and Pd-Z-K-R samples become significantly more pronounced compared to the poisoned samples, suggesting a notable re-emergence of divalent Pd^{2+} species, including $Pd(OH)^+$ and Pd^{2+} cations, in the regenerated catalysts.

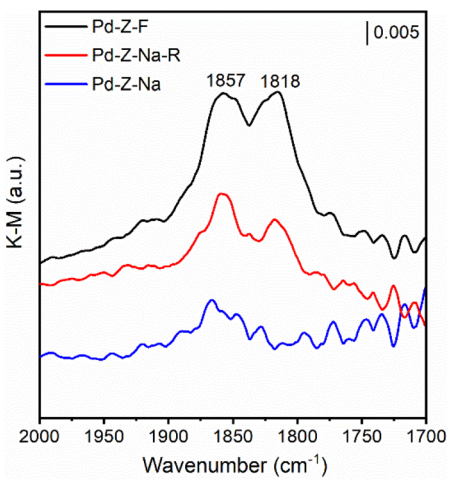

Fig. 7 NO-DRIFTS profiles of Pd-Z-F, Na poisoned Pd-Z-Na and the regenerated Pd-Z-Na-R catalysts.

NH_3-DRIFTS serves as a potent analytical tool for probing the interaction between metal cations (*e.g.*, Pd^{2+} and Cu^{2+}) and the zeolite framework.[9,27,42,43] It has been well-established that FT-IR bands in the 1000–850 cm^{-1} range reflect the T–O–T vibrations of the zeolite framework, which are perturbed by Cu^{2+} ions.[27,42,44] A similar disruption of T–O–T vibrations induced by exchanged Pd ions was observed in Pd-SSZ-13, a finding that was unequivocally corroborated through *in situ* NH_3-DRIFTS analysis.[9,43] As depicted in Fig. 8a, S15a and S16, the IR spectrum of the Pd-Z-F catalyst reveals two prominent peaks at 872 and 903 cm^{-1}, corresponding to Pd^{2+} and $Pd(OH)^+$ species in 6MR and 8MR, respectively.[9,43] Upon poisoning, these peaks at 872 and 903 cm^{-1} nearly vanish, signifying that the introduction of Na and K leads to a significant depletion of active Pd^{2+} and $Pd(OH)^+$ cations. Notably, these peaks attributable to isolated Pd^{2+} and $Pd(OH)^+$ species are partially restored following treatment with a dilute NH_4Cl solution. This alteration in the Pd states is likely ascribed to the ability of NH_4^+ ions in the NH_4Cl solution to facilitate the transformation of PdO species, which are initially formed due to alkali-metal poisoning, back into their active Pd^{2+} counterparts. Additionally, as indicated in Fig. 8b, S15b and S17, NH_3-DRIFTS was also employed to investigate the OH vibrational (νOH) region of the catalysts, providing insight into the modifications of hydroxyl groups within the Pd-SSZ-13 framework.[31,32,34,45] Thus, NH_3 adsorption DRIFTS measurements were conducted to assess the impact of Na or K poisoning and the subsequent regeneration process on the hydroxyl groups within Pd-SSZ-13 catalysts. As shown in Fig. 8b and S15b, four distinct νOH features at 3737, 3668, 3619, and 3588 cm^{-1} were identified in the Pd-Z-F catalyst. As is known that the bands at 3737 and 3668 cm^{-1} are attributed to terminal Si–OH and $Pd(OH)^+$ species, respectively, while the peaks at 3619 and 3588 cm^{-1} corresponded to Brønsted acid sites (*i.e.*, Si–O(H)–Al) remain unoccupied by positively charged Pd^{2+} ions.[9,34,45] Following poisoning, the band at 3668 cm^{-1}, associated with $Pd(OH)^+$ species, almost completely disappeared due to the exchange of alkali-metal ions into the ion-exchange sites in CHA cages. Furthermore, the majority of Brønsted acid sites became occupied by alkali-metal ions, leading to a marked reduction in the peaks at 3619 and 3588 cm^{-1} in the poisoned Pd-Z-Na and Pd-Z-K samples. Remarkably, the peak at 3668 cm^{-1}, representing $Pd(OH)^+$ species, reappeared post-regeneration with NH_4Cl solution. This indicates that the PdO species can be effectively converted back to divalent Pd^{2+} species. Additionally, the intensities of the peaks at 3619 and 3588 cm^{-1} in the regenerated Pd-Z-Na-R and Pd-Z-K-R catalysts were significantly stronger than in the poisoned samples. These findings conclusively demonstrate that the Brønsted acid sites in SSZ-13 can be effectively reinstated through the removal of alkali-metal ions from the catalyst *via* NH_4Cl washing.

3.3 Proposed mechanism of alkali-metal-induced deactivation and regeneration of Pd-SSZ-13

The deactivation of Pd-SSZ-13 catalysts induced by alkali metals and the subsequent regeneration mechanism following NH_4Cl

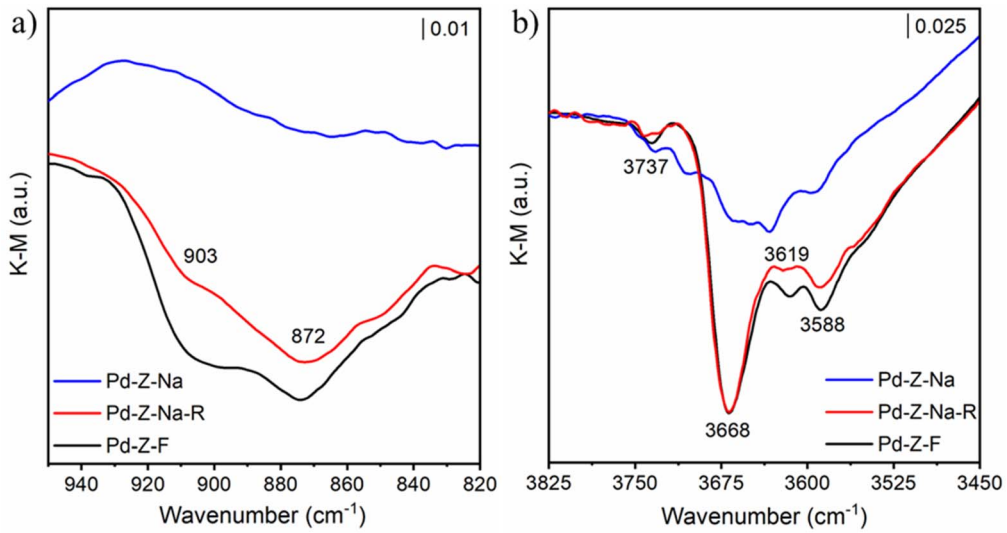

Fig. 8 NH_3-DRIFTS profiles of Pd-Z-F, Na poisoned Pd-Z-Na and the regenerated Pd-Z-Na-R catalysts: (a) T–O–T regions; (b) OH vibrational region.

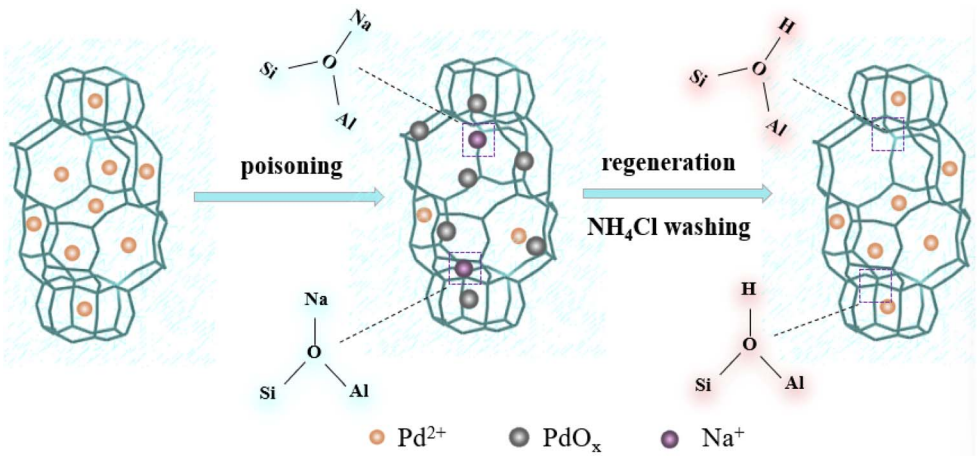

Fig. 9 Schematic illustration of the Na-induced deactivation and subsequent regeneration mechanism of the poisoned Pd-SSZ-13 catalysts following NH_4Cl washing.

washing is comprehensively elucidated, as illustrated in Fig. 9. Upon careful analysis of the experimental results and associated discussion, it is evident that the effect on the CHA framework of Pd-SSZ-13 resulted by alkali metals is negligible. However, alkali metals, such as Na, exert a detrimental effect on the active isolated Pd^{2+} sites and Brønsted acid sites, thereby significantly reducing the adsorption efficacy of the poisoned Pd-SSZ-13. Specifically, the incorporation of Na leads to the displacement of Pd active sites from their ion-exchange locations, resulting in pronounced aggregation of Pd species and the formation of non-active PdO particles. In addition, Na^+ ions can interact with Brønsted acid sites, replacing H^+ ions to form Si–O(Na)–Al linkages, thereby diminishing the surface acidity of the zeolite. Crucially, the NH_4Cl washing treatment promotes the redispersion of Pd species, thereby alleviating both the physical and chemical deactivation of Pd-SSZ-13. Furthermore, this washing process facilitates the recovery of Brønsted acid sites by effectively removing the Na^+ species that have accumulated on the catalyst surface.

4 Conclusions

In this study, a facile and highly effective methodology was employed to regenerate Pd-SSZ-13 catalysts poisoned by alkali metals, utilizing a dilute NH_4Cl solution washing. The mechanisms of alkali metal-induced poisoning and subsequent regeneration were elucidated through an extensive suite of *ex situ* physicochemical characterizations and *in situ* DRIFTS analysis. It was observed that alkali metal poisoning leads to a significant decline in the NO_x adsorption capacity of Pd-loaded SSZ-13 zeolite catalysts, as alkali metals not only occupy the Brønsted acid sites but also promote the transformation of active Pd^{2+} into PdO aggregates. Notably, washing with NH_4Cl solution not only reverts the inactive PdO_x species

to Pd^{2+} ions but also facilitates the removal of alkali metals, thereby restoring the Brønsted acid sites. This discovery unveils a straightforward yet potent method for regenerating Pd-loaded zeolites that have been poisoned by alkali metals, thereby offering a promising strategy for the recovery of Pd-loaded zeolites subjected to other chemical poisons (*e.g.*, P and S) and significantly extending their operational lifespan in practical applications.

Author contributions

Dongdong Chen: writing – original draft & editing, investigation, data curation, project administration, funding acquisition. Weiqi Zhang: writing – original draft, data curation. Zhenzhen Jia: data curation, conceptualization, methodology. Huibin Liu: data curation. Bo Zhang: writing – review & editing, investigation. Shasha Liu: investigation, funding acquisition. Feng Liang: data curation. Wuwan Xiong: data curation. Xiang Li: conceived the idea, designed the study, writing – review & editing.

Conflicts of interest

The authors declare no conflict of interest.

Data availability

The data that support the findings of this study are available from the corresponding author, upon reasonable request.

Supplementary information (SI): additional PNA performances, N_2-physisorption information, XRD patterns, DR UV/Vis spectra, TEM (and HAADF-STEM images), EDX mappings, high-resolution XP Na 1s and K 2p spectra, H_2-TPR curves and NH_3-TPD profiles, NO- and NH_3- DRIFTS of the K-poisoned Pd-Z-K and the regenerated Pd-Z-K-R catalysts; representative FE-SEM images, EDX mappings (Al, Si and O), time-resolved *in situ* NO- and NH_3- DRIFT of the Pd-Z-F, alkali-metal poisoned Pd-Z-Na and Pd-Z-K, the regenerated Pd-Z-Na-R and Pd-Z-K-R catalysts. See DOI: https://doi.org/10.1039/d5ra08741d.

Acknowledgements

This study was generously funded by the National Natural Science Foundation of China (22306155), the Guangdong University Innovation Project (2024KTSCX032), the Zhaoqing University Natural Science Project (ZD202408, qn202526), Funded Project for Innovative Scientific Research Teams of Zhaoqing University (TD202418) and Innovative Entrepreneurship Project of Chinese College Students (X202510580134, 202410580016, 202410580017, 202410580018).

References

1 Z. Liu, M. Shen, S. Wang, C. Zhang, G. Shen, X. Li, W. Li and F. Gao, *J. Catal.*, 2026, **453**, 116459.
2 Y. Yue, S. Xiong, H. Ou, Y. Yang, X. Sun, H. Wang, Y. Xi, Z. Gong, J. Chen and J. Li, *Appl. Catal., B*, 2026, **380**, 125753.
3 Q. Zhou, B. Zhu, Y. Wang, Z. Zhang, X. Mao, M. Tao, H. Zhang and C. Tang, *Appl. Catal., B*, 2026, **381**, 125881.
4 D. Chen, A. Khetan, H. Lei, V. Rizzotto, J.-Y. Yang, J. Jiang, Q. Sun, B. Peng, P. Chen, R. Palkovits, D. Ye and U. Simon, *Environ. Sci. Technol.*, 2023, **57**, 16121–16130.
5 F. Gao, D. Mei, Y. Wang, J. Szanyi and C. H. F. Peden, *J. Am. Chem. Soc.*, 2017, **139**, 4935–4942.
6 C. Paolucci, I. Khurana, A. A. Parekh, S. Li, A. J. Shih, H. Li, J. R. Di Iorio, J. D. Albarracin-Caballero, A. Yezerets, J. T. Miller, W. N. Delgass, F. H. Ribeiro, W. F. Schneider and R. Gounder, *Science*, 2017, **357**, 898.
7 H. Wu, X. Dai, W. Teng, J. Li, Y. Chen, C. Ding, S. Ren and J. Yang, *J. Alloys Compd.*, 2025, **1034**, 181351.
8 Z. Pei, H. Wang, H. Zhao, J. Xu, C. He and Z. Ji, *J. Alloys Compd.*, 2024, **1008**, 176533.
9 D. Chen, H. Lei, W. Xiong, Y. Li, X. Ji, J.-Y. Yang, B. Peng, M. Fu, P. Chen and D. Ye, *ACS Catal.*, 2021, **11**, 13891–13901.
10 D. Li, Q. Ding, Y. Meng, Y. Guo, L. Pang and T. Li, *Sep. Purif. Technol.*, 2023, **322**, 124344.
11 H.-Y. Chen, J. E. Collier, D. Liu, L. Mantarosie, D. Durán-Martín, V. Novák, R. R. Rajaram and D. Thompsett, *Catal. Lett.*, 2016, **146**, 1706–1711.
12 K. Khivantsev, N. R. Jaegers, L. Kovarik, J. C. Hanson, F. Tao, Y. Tang, X. Zhang, I. Z. Koleva, H. A. Aleksandrov, G. N. Vayssilov, Y. Wang, F. Gao and J. Szanyi, *Angew. Chem., Int. Ed.*, 2018, **57**, 16672–16677.
13 K. Mandal, Y. Gu, K. S. Westendorff, S. Li, J. A. Pihl, L. C. Grabow, W. S. Epling and C. Paolucci, *ACS Catal.*, 2020, **10**, 12801–12818.
14 C. Gao, H. Wang, B. Zhou, B. Wang, R. Wang, Y. Long, D. Wang, Y. Peng and J. Li, *Commun. Eng.*, 2024, **3**, 164.
15 Y. Li, D. Chen, X. Xu, X. Wang, R. Kang, M. Fu, Y. Guo, P. Chen, Y. Li and D. Ye, *Environ. Sci. Technol.*, 2023, **57**, 3467–3485.
16 X. Li, F. Gao, W. Li, M. Shen, J. Wang and G. Shen, *J. Environ. Chem. Eng.*, 2024, **12**, 113468.
17 C. Fan, J. Mi, Q. Wu, J. Chen and J. Li, *Processes*, 2022, **10**, 222.
18 H. Cheng, X. Tang, H. Yi, Y. Yao, Y. Wang, Z. Li, X. Ren, F. Gao, Y. Zhou, L. Bao and Q. Yu, *Sep. Purif. Technol.*, 2025, **356**, 129962.
19 J. Cai, Y. Huang, X. Wu, Z. Huang, H. Shen, K. Cui, Z. Li, G. Jing, J. W. Schwank and H. Zhao, *Chem. Eng. J.*, 2023, **478**, 147399.
20 C. Wang, X. Kang, Y. Gu and F. Gao, *Chem. Eng. J.*, 2025, **503**, 158299.
21 X. Chen, M.-Y. Nan, J. Huang, L. Li, Z. Zhang and G. Yang, *Environ. Sci. Technol.*, 2025, **59**, 20546–20556.
22 N. Kang, Y. Wang, J. He, Y. Wang, X. Guo, H. Qu, T. Zhang, C. Zhang, M. Yan and P. Xie, *Chem. Eng. J.*, 2025, **516**, 164041.
23 Y. Cui, Y. Wang, D. Mei, E. D. Walter, N. M. Washton, J. D. Holladay, Y. Wang, J. Szanyi, C. H. F. Peden and F. Gao, *J. Catal.*, 2019, **378**, 363–375.
24 D. Li, Q. Ding, D. Hao, J. Han, G. Yang, L. Pang, Y. Guo, J. Yu and T. Li, *Environ. Sci. Technol.*, 2023, **57**, 19956–19964.

25 J. Lee, Y. Ryou, S. J. Cho, H. Lee, C. H. Kim and D. H. Kim, *Appl. Catal., B*, 2018, **226**, 71–82.
26 T. M. Lardinois, J. S. Bates, H. H. Lippie, C. K. Russell, J. T. Miller, H. M. Meyer III, K. A. Unocic, V. Prikhodko, X. Wei, C. K. Lambert, A. B. Getsoian and R. Gounder, *Chem. Mater.*, 2021, **33**, 1698–1713.
27 X. Hu, J. Lin, X. Tan, C. Lin, Y. Zhang and W. Shan, *Chem. Eng. J.*, 2025, **520**, 165978.
28 X. Hu, J. Lin, X. Tan, C. Lin, H. Zhang, Y. Zhang and W. Shan, *Chem. Eng. J.*, 2025, **510**, 161874.
29 S. Zhang, J. Tan, Y. Meng, X. Tang, Y. Shan, J. Du, D. Xia, W. Cai and T. Li, *Chem. Eng. J.*, 2025, **506**, 160054.
30 T. Usui, Z. Liu, S. Ibe, J. Zhu, C. Anand, H. Igarashi, N. Onaya, Y. Sasaki, Y. Shiramata, T. Kusamoto and T. Wakihara, *ACS Catal.*, 2018, **8**, 9165–9173.
31 X. Tang, Y. Gao, W. Li, S. Dai, L. Wang, Y. Guo, Y. Guo, W. Zhan and A. Wang, *Environ. Sci. Technol.*, 2025, **59**, 13447–13457.
32 H. Zhao, X. Chen, A. Bhat, Y. Li and J. W. Schwank, *Appl. Catal., B*, 2021, **286**, 119874.
33 C. Wang, X. Kang and F. Gao, *Chem. Eng. Sci.*, 2025, **316**, 121923.
34 L. Liu, W. Xiong, M. Fu, J. Wu, Z. Li, D. Ye and P. Chen, *Chin. Chem. Lett.*, 2024, **35**, 108870.
35 Y. Ryou, J. Lee, H. Lee, C. H. Kim and D. H. Kim, *Catal. Today*, 2019, **320**, 175–180.
36 Y. Shen, W. Dong, L. Zhang, L. Wang, B. Chen, Y. Guo, W. Zhan, A. Wang, C. Ge and Y. Guo, *Sep. Purif. Technol.*, 2024, **330**, 125248.
37 Y. Wang, X. Shi, Y. Shan, J. Du, K. Liu and H. He, *Ind. Eng. Chem. Res.*, 2020, **59**, 6416–6423.
38 F. Gao, Y. Wang, N. M. Washton, M. Kollár, J. Szanyi and C. H. F. Peden, *ACS Catal.*, 2015, **5**, 6780–6791.
39 V. Mesilov, B. Zhuang, S. Xi and S. L. Bernasek, *J. Phys. Chem. C*, 2023, **127**, 11490–11505.
40 K. Khivantsev, N. R. Jaegers, L. Kovarik, M. Wang, J. Z. Hu, Y. Wang, M. A. Derewinski and J. Szanyi, *Appl. Catal., B*, 2021, **280**, 119449.
41 A. Wang, K. Lindgren, M. Di, D. Bernin, P.-A. Carlsson, M. Thuvander and L. Olsson, *Appl. Catal., B*, 2020, **278**, 119315.
42 D. Chen, Y. Yan, A. Guo, V. Rizzotto, H. Lei, Z. Qiao, H. Liang, M. Jabłońska, X. Jiang, J. Jiang, R. Palkovits, P. Chen, D. Ye and U. Simon, *Appl. Catal., B*, 2023, **322**, 122118.
43 H. Zhao, X. Chen, A. Bhat, Y. Li and J. W. Schwank, *Appl. Catal., B*, 2021, **282**, 119611.
44 J. Lin, X. Hu, X. Tan, Y. Zhang, C. Lin, W. Shan and H. He, *Environ. Sci. Technol.*, 2025, **59**, 1864–1874.
45 J. Zhang, Q. Dong, T. Zhang, G. Ma, Y. Zhang, J. Zhao, J. Liu and J. Li, *Appl. Catal., B*, 2024, **357**, 124359.